Ore Geology Reviews 99 (2018) 411–424

Contents lists available at ScienceDirect

Ore Geology Reviews

journal homepage: www.elsevier.com/locate/oregeorev

Selenium and tellurium resources in Kisgruva Proterozoic volcanogenic massive sulphide deposit (Norway)

Liam A. Bullock[a,b,*], Magali Perez[c], Joseph G. Armstrong[a], John Parnell[a], John Still[a], Joerg Feldmann[c]

[a] School of Geosciences, University of Aberdeen, Aberdeen AB24 3UE, UK
[b] Ocean and Earth Science, National Oceanography Centre Southampton, University of Southampton, Southampton SO17 1BJ, UK
[c] Trace Element Speciation Laboratory (TESLA), Department of Chemistry, University of Aberdeen, Aberdeen AB24 3UE, UK

ARTICLE INFO

Keywords:
Selenium
Tellurium
Sulphide ore
Pyrite
VMS
Norway

ABSTRACT

The former mining site at Kisgruva near Kongsberg, Norway, is primarily composed of worked sulphide ore deposits, of hydrothermal origin, which occur within Precambrian metamorphic basement. Though the original targets at the Kisgruva mine site were extraction of copper (Cu), sulphur (S) and iron (Fe), the sulphide ore also contains exceptionally high concentrations of selenium (Se) and tellurium (Te), hosted within selenides (clausthalite and minor naumannite) and tellurides (hessite and minor altaite and tellurobismuthite). Both Se and Te are also present within the sulphide ore in pyrite and chalcopyrite, which contain exceptionally high concentrations of up to 688 ppm Se and 81 ppm Te. Additionally, oxidative weathering of the exposed bedrock has resulted in the accumulation of hyper-enriched, unconsolidated weathered crust deposits at surface (Se up to 1590 ppm; Te up to 63 ppm), containing selenite (SeO_3^{2-}) and tellurite (TeO_3^{2-}) ions. Concentrations of Se and Te are subsequently higher in the weathering products than in the sulphide ore, due to fixation on to organic matter (~0.4% in weathered ore crusts), jarosite (formed from oxidation of sulphides from the primary ore), ferric oxide and hydroxide phases (goethite and haematite). Increasing demand for Se and Te to use in green technologies has led to the reassessment of these orebodies and their associated weathered ore crust deposits. Though these elements are currently considered mining contaminants, this and similar sites may be of future economic importance, particularly as demand for Se and Te continues to rise.

1. Introduction

A greater knowledge of how critical element such as selenium (Se) and tellurium (Te) concentrate and are spatially distributed in solid ore rock and the associated weathered profile is of increasing economic importance. This is particularly relevant as the worldwide demand for viable sources of Se and Te continue to grow. The former Kisgruva sulphide mine in the Kongsberg region of Buskerud (Norway) is known to host high Se and Te concentrations, though well-constrained data from the region are limited (NGU, 1981, 2017; Bjerkgård, 2015; Kotková et al., 2018). This is in part due to the historically low economic importance of Se and Te. Concentrated Se from ore extraction activities is presently considered toxic, particularly relating to its liberation and release from mining sites (Lemly, 2004; Sandy et al., 2010; Khamkhash et al., 2017). Tellurium is also toxic in high concentrations (Pohl, 2011; Schirmer et al., 2014), particularly in the form of tellurite (TeO_3^{2-}; Templeton et al., 2000; El-Shahawi et al., 2013). However, in recent years, Se and Te have become critical 'E-tech' elements, used in alloys, photovoltaic products and nanotechnologies (Ba et al., 2010; Belzile and Chen, 2015; Jin et al., 2016; Wei et al., 2016), and minerals such as pyrite should be considered a potential source of economic interest for these elements (Keith et al., 2017). The growing necessity for sources of E-tech elements has led to an increasing focus on new potential concentrated Se and Te deposits and a review of former ore mining sites, such as the Kisgruva site.

The Kisgruva site is part of the greater Kongsberg mining region (Fig. 1). Vein deposits in banded diorite, granitic gneiss and amphibolite have been extensively worked in the Kongsberg region for Cu and Ag deposits for over five centuries (Bugge, 1917, 1928, 1937; NGU, 1981, 2017). This metamorphic sequence follows the north-south parallel regional 'fahlbands', which are subvertical zones enriched in sulphides of hydrothermal origin (Bugge, 1917, 1928, 1937; Gammon, 1966; Boyle, 1968; Kotková et al., 2018). To the south of Kongsberg, a more sporadic distribution of sulphide deposits has been worked on a

* Corresponding author.
E-mail address: liam.bullock@abdn.ac.uk (L.A. Bullock).

https://doi.org/10.1016/j.oregeorev.2018.06.023
Received 26 March 2018; Received in revised form 22 June 2018; Accepted 28 June 2018
Available online 07 July 2018

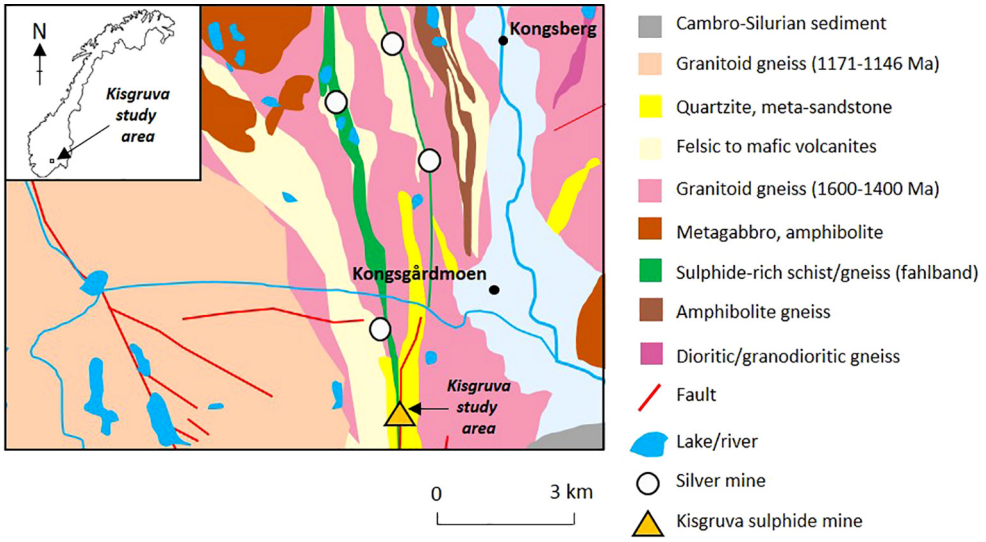

Fig. 1. Geological map and sampling location in the Kisgruva area of the Kongsberg mining region (modified after Viola et al., 2016; Kotková et al., 2018).

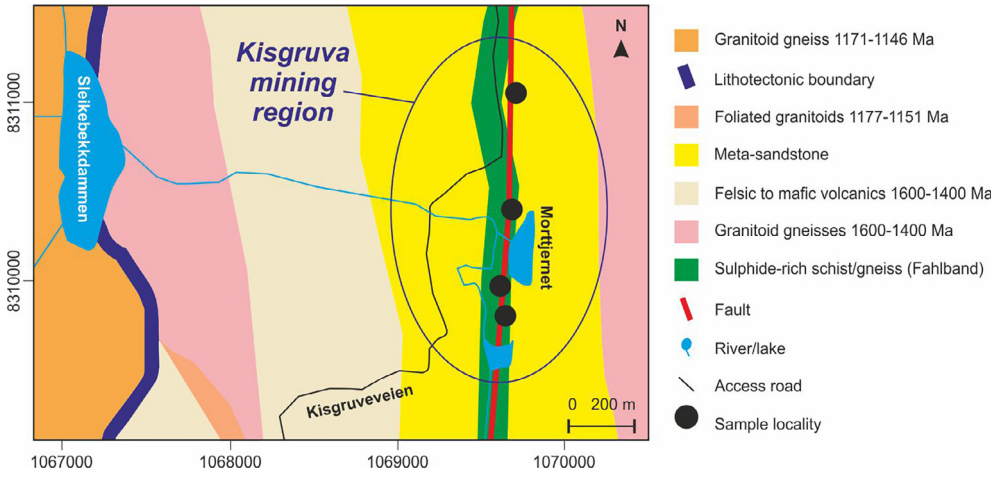

Fig. 2. Sampling sites and local geology in the Kisgruva mining region (modified after Viola et al., 2016; Kotková et al., 2018).

smaller scale, including the Kisgruva deposit (Bugge, 1928; NGU, 1981, 2017; Fig. 1). Former Kisgruva workings are now characterised by exposure of extensively worked sulphide ore deposits, the metamorphic bedrock host and the outermost weathered sulphide ore crust. A potentially key Se (and by chemical association, Te) source in near-surface environments is an oxidation zone of Se and Te-bearing mineral phases, sulphide deposits and associated waste products (Charykova and Krivovichev, 2017), meaning sites such as Kisgruva may host potentially high Se in both primary ore deposits and their weathered derivatives. Secondary formation of Se and Te-bearing mineral phases is caused by active precipitation of aqueous solutions in near-surface conditions within the oxidation zone of sulphide ores, under conditions of seasonal fluctuations of temperatures and atmospheric pressure (~1 bar) (Charykova and Krivovichev, 2017). Elements such as Se and Te may be mobilised under oxidising conditions (Howard, 1977; Northrop and Goldhaber, 1990; Simon et al., 1997; Xiong, 2003; Min et al., 2005; Spinks et al., 2014, 2016), and re-precipitated in the presence of a reducing agent (e.g. carbonaceous materials, sulphides, biogenic H_2S, ferromagnesian minerals; Spinks et al., 2014, 2016). These elements may be co-precipitated with iron oxides and adsorbed from solution (Parnell et al., 2018).

Despite a handful of reports and studies which refer to high Se in the region (NGU, 1981, 2017; Bjerkgård, 2015; Kotková et al., 2018), the mineralogy and trace element geochemistry of Kisgruva sulphide ore deposits, metamorphic bedrock and weathered ore crust is relatively unknown. Therefore, the aims of this study are to:

- Obtain an overview of Se and Te concentrations in Kisgruva sulphide ore, bedrock and weathered ore crust.
- Identify mineral hosts and speciation of Se and Te at Kisgruva.
- Determine the processes of Se and Te mobility and fixation at Kisgruva.
- Review the economic potential of the Kisgruva site for Se and Te.

Sampled deposits include (1) the mineralised sulphide ore zones, (2) the crystalline metamorphic bedrock host, and (3) the outermost weathered crust of the ore. Sample mineralogy, whole rock Se and Te concentrations and Se and Te speciation were determined for sulphide ore and weathered ore crust deposits. High Se and Te deposits in Kisgruva offer an opportunity to assess the means of occurrence, origins, transport mechanisms and enrichment of these critical elements. Sulphide ores and associated weathered ore crusts at Kisgruva and similar sites former mining sites may provide a key source of Se and Te, important as demand continues to increase worldwide.

2. Historic mining at Kisgruva

The former Kisgruva mine (Figs. 1 and 2) has an estimated 581

thousand tons of reserves, with 50 thousand tons produced during operations, and 3200 m^3 volume of dump remaining (NGU, 1981, 2017). The Kisgruva deposit was predominantly worked for Cu, grading up to 1.55% (Bugge, 1928), and for sulphides for use in Ag smelting processes in the nearby town of Kongsberg (Fig. 1). Operations commenced at Kisgruva in 1650, with regular production finishing in 1902. Since 1944, the site has seen sporadic activity and exploration, including geophysical surveying, core drilling and inspections (NGU, 1981, 2017).

Drilling in the 1950s identified potentially ore grade materials, including 1.01% Cu, 1.18% Zn, 19.5% S, 430 g/t Se, 25 g/t Ag and 2.5 g/t Au. High Se was confirmed in the 1980's, but Au content could not be validated (NGU, 1981, 2017). The mine today is predominantly water filled. During surveying by the Norwegian Institute for Water Research in 2001–2002, water samples were taken at Kisgruva (NIVA, 2003). Water sample results showed that mining activities produced a highly acidic drainage, with a pH of approximately 2.7. Iron (Fe) is the most important heavy metal in drainage water (up to 66.6 mg/l), as well as SO_4 (572 mg/l) (NIVA, 2003). Concentrations of Ca, Mg, Al, Cu, Zn, Cd, Pb, Mn, Ni, Co and Si were also measured. With the exceptions of Fe and SO_4, results indicated that Cu and other measured metal contaminations were low. If an annual rainfall is assumed, coupled with an average concentration of Cu of 3 mg/l and a medium water drainage at 1 l/s, the annual Cu transport from the area was estimated at ~90 kg (NIVA, 2003).

3. Geological setting

The Kisgruva area forms part of the Kongsberg gneiss complex of island arc volcanosedimentary sequences and plutonic rocks (1570–1500 Ma, Andersen et al., 2004), affected by Sveconorwegian deformation and amphibolites facies metamorphism (Bingen et al., 2008b). The Kisgruva region is characterised by metamorphic rocks, with Cambro-Silurian sediments to the south east (Figs. 1 and 2). The Kisgruva area and greater Kongsberg region has undergone a sustained history of deformation and metamorphism, with periods of deposition and igneous activity, summarised in Table 1 and here (for a more comprehensive summary, see Starmer, 1985; Andersen et al., 2004; Bingen et al., 2008a, b; Bjerkgård, 2012). Following the initial period of deposition and volcanism (~1700–1600 Ma), the Kongsberg region underwent amphibolite-granulite facies metamorphism (under approximate conditions of 700–800 °C and 6–8 kbar). This produced a zone of folded and sheared metasediments and granitic gneisses (formed 1700–1500 Ma), metamorphosed and deformed during the Kongsbergian orogeny (1600–1450 Ma) (Starmer, 1985; Andersen et al., 2004; Bjerkgård, 2012). This was followed by further intrusive activity and associated deformation, before a second phase of metamorphism reached greenschist to amphibolite facies metamorphism during the Sveconorwegian Orogeny (~1110–1080 Ma) (Starmer, 1985; Bingen et al. 2008b).

Table 1
Major geological events affecting the Kisgruva area and greater Kongsberg region. Conditions (episodes of activity) and events shown in relative chronological order (from oldest to youngest) (Adapted from Starmer, 1985).

Dates (Ma)	Conditions	Events
~1700–1600	Deposition Volcanism Subsidence	Shelf sediments overlain by deeper water sediments and intermediate volcanics; sulphidic layers developed; sinking of region
~1550–1500 (Kongsbergian Orogeny)	Deformation Intrusive activity	Compression of quartzite and various gneisses; granitic intrusions; granulite facies metamorphism (mantle degassing); thrusting; gabbro-diorite-tonalite intrusions; thrusting
~1390–1200 (Sveconorwegian Orogeny)	Intrusive activity Deformation	Granitic intrusions; gabbroic intrusions; dislocation; granitic intrusions; thrusting
~1200–1000 (Sveconorwegian Orogeny)	Intrusive activity Metamorphism Deformation Deposition Volcanism Subsidence	Gabbroic intrusions; amphibolite facies metamorphism; uplift; shallow water sediment deposition and volcanics; sinking of region; dolerite intrusions; thrusting; granitic intrusions; epidote amphibolite facies metamorphism; faulting; granitic intrusions
~970–900	Uplift Deformation	Granitic intrusions; faulting

The Kisgruva deposit forms part of the regional fahlbands. The sulphide-bearing fahlbands form concordant layers throughout the Western Kongsberg Complex and Eastern Kongsberg Complex, which contain variable quartz-plagioclase-biotite-hornblende gneisses (Starmer, 1985). These variable gneisses show chemical composition characteristics of dacitic-andesitic volcanics and greywackes, reflecting their mixed volcanic-sedimentary origin (Starmer, 1985). The crystalline bedrock was formed ~ 1400–1500 Ma, intruded by 1160–70 Ma granitoids (Bingen et al., 2008a; Scheiber et al., 2015). The fahlbands trend subparallel to the foliation of the surrounding lithologies, and are strongly deformed, suggesting formation prior to the regional deformation and metamorphism (Gammon, 1966; Kotková et al., 2018). Sulphide ores within the metamorphic basement occur as occasional lenses up to 1 m in length, consisting of pyrite, chalcopyrite and pyrrhotite (Gammon, 1964; NGU, 2017; Kotková et al., 2018). Sulphides also occur as disseminated individual crystals which define the foliation of the bedrock host, wrapped by mica (Gammon, 1964).

The origin of the impregnated sulphide lenses is debated. Early researchers favoured the notion that sulphide deposition related to mafic intrusive activity, followed by regional metamorphism (Kjerulf and Dahll, 1861; Helland, 1879; Vogt, 1899; Bugge, 1917), while later research suggested a volcanic exhalative sea floor (VMS) origin (Gammon, 1966; Starmer, 1977; Bjerkgård, 2015), precipitation along fractures (Sverdrup et al., 1967) or a combination of these geological processes (Bancroft et al., 2001). The typical lens-like shape of Kisgruva suggests a probable VMS formation due to venting of hydrothermal solutions. Exposed (previously worked) regions of primary sulphide ore deposits have been subjected to prolonged periods of weathering, resulting in the development of a rust-like weathered ore crust. This weathered ore crust developed due to the weathering of pyrite and pyrrhotite, which predominantly comprise the ore, as well as subordinate to accessory phases such as chalcopyrite, sphalerite, galena, arsenopyrite and cobalt-bearing minerals (Bjerkgård, 2012; NGU, 2017).

4. Materials and methods

Metamorphic bedrock (n = 4), sulphide ore (n = 6) and weathered ore crust (n = 6) samples were collected in-situ from the former Kisgruva mining site (Fig. 2). Samples were analysed and characterised by mineralogical and geochemical methods. Previously worked sulphide ore exposures occur sporadically over a transect distance of ~0.65 km, with four prominent worked regions of ~20–30 m^2 ground coverage. Samples were collected from each of the four identified sites to ensure full spatial coverage was achieved. Weathered ore crusts are generally restricted to 1–2 m^2 on top of sulphide ore exposures. Fresh (unweathered) metamorphic bedrock and sulphide ore samples were collected from each site, and weathered ore crust samples were taken from the centre of the limited exposures.

4.1. Scanning electron microscopy

Whole rock samples were examined using a Zeiss Gemini300 VP FEG Scanning Electron Microscope (SEM) with energy-dispersive X-ray

spectroscopy detector facility at the University of Aberdeen for mineralogical determination in sulphide ore and metamorphic basement samples.

4.2. X-ray diffraction

X ray diffraction (XRD) was performed on weathered Kisgruva weathered ore crust samples to determine individual mineralogical and compositional phases that otherwise cannot be determined by SEM. The finely-powdered (< 64 μm) samples were placed on a flat disk sample holder, gently compressed and scanned on a Bruker D8 Discover diffractometer at the University of Aberdeen, using CuKα radiation and a scan range from 5 to 90° (2 Theta), a 0.03° (2 Theta) step size and a data collection time of 10 s per step. Interplanar spacing was calculated using Bragg's Law (d) = (n) × (λ) ÷ 2 × Sinθ, where d = interplanar spacing, n = order of reflection and λ = wavelength (Bragg, 1912). Reference data identified from Anthony et al. (1990), Downs and Hall-Wallace (2003) and Lafuente et al. (2015).

4.3. Whole rock geochemistry

Whole rock samples were analysed for Se and Te and associated chalcophile elemental concentrations by both inductively coupled plasma atomic emission spectroscopy (ICP-AES) and solution ICP-MS. Samples of ~30 g were individually milled and homogenised, and 0.5 g were digested with aqua regia in a graphite heating block. The residue was diluted with deionised water (18 MΩ cm), mixed, and analysed using a Varian 725 instrument (ALS Minerals, OMAC Laboratories, Loughrea; method ID: ME-MS41). Results were corrected for spectral inter-element interferences from the sample matrix, solvent medium and plasma gas. Errors for whole rock for ICP-MS were calculated based on certified and achieved values for certified reference materials (CRM). Results for CRM analysis were within the anticipated target range for each metal and standard. Duplicate analyses produced reported values within the acceptable range for laboratory duplicates, with an average relative percent difference of 4%. Total organic carbon (TOC) and S contents were measured using a LECO CS225 elemental analyser at the University of Aberdeen. Analyses were run concurrently with standards 501-024 (Leco Instruments, instrument uncertainty ± 0.05% C, ± 0.002% S) and BCS-CRM 362. The repeatability, based on 3 repeats of CRMs and blanks, was consistently within 1%.

4.4. Laser ablation

Trace element analysis of polished sulphide ore blocks of generally inclusion-free pyrite was performed by using a New Wave laser ablation system UP213 nm coupled to an ICP-MS Agilent 7900 at the University of Aberdeen. The laser beam was fired with a spot size of 100 μm, a 10 Hz repetition rate and at 50 μm s^{-1} ablation speed with 1 J cm^2 energy. Before ablation, a warm-up of 15 s was applied, with 15 s delay between each ablation. Parameters were optimised using a NIST Glass 612 to obtain the maximum sensitivity and to ensure low oxide formation. To remove possible interferences which could affect Se measurement, a reaction cell was used with hydrogen gas, between 3.0 and 3.5 mL/min optimisation to decrease Se background. MASS-1 synthetic polymetal sulphide (US Geological Survey) and FeS^{-1} (Slim Group, University of Quebec) CRMs were used to provide quantification. For that, an external calibration was plotted for each element by using the two CRMs and a background value of 0 ppm.

4.5. Sequential extraction and speciation

Sequential extraction and speciation was performed on Kisgruva weathered ore crust samples to determine the pH and the total concentration of Se and Te species adsorbed onto oxide minerals and organic matter. The general principle of the extraction has been reported in several scientific articles, such as Kulp and Pratt (2004) and Di Tullo et al. (2016). A phosphate buffer extraction was undertaken to give the total concentration and speciation of Se and Te adsorbed to charged surfaces as oxide minerals, while extraction with sodium hydroxide was conducted to give concentration and speciation adsorbed to organic matter. Aqua regia residues were used to indicate the total unextractable concentrations of Se and Te. The pH was assessed by shaking 4 g of each sample in 20 mL of deionised water. After 20 min, the samples were centrifuged at 3500 rpm for 3 min and the pH was measured in the supernatant.

The samples were crushed and dried, with 0.5 g dissolved in a 10 mL phosphate buffer solution and prepared with potassium phosphate monobasic purchase from Sigma Aldrich (0.1 mmol L^{-1}, pH 7). To measure the elemental form of Se and Te, 1 mol L^{-1} of sodium sulphite (Acros Organics) was added to the phosphate buffer solution. The samples were shaken for 2 h, then centrifuged at 3500 rpm for 3 min. Supernatants were collected and stored at 4 °C before speciation and total concentration measurements. The pellet obtained after phosphate extraction were extracted in 10 mL of 0.1 mol L^{-1} sodium hydroxide (Fisher Chemical) for 2 h at 90 °C. Samples were then centrifuged, supernatants were collected and stored at 4 °C before analysis. Finally, the residues remaining from extraction were digested by aqua regia. The aqua regia solution was prepared with 2 mL of 70% nitric acid and 6 mL of hydrochloric acid (both obtained from Fisher Chemical). Three replicates were performed for each sample.

4.6. Speciation and total concentration analysis

All analyses were performed with an ICP-MS 7900, coupled to a HPLC 1100 (Agilent Technology, Japan). A Hamilton PRP-100 column was used with a phosphate buffer as a mobile phase (1 mL min^{-1}). The buffer solution was prepared with potassium phosphate monobasic purchase from Sigma Aldrich (10 mmol L^{-1}) and the pH was adjusted to 10 by using an ammonia solution. The volume of samples injected was 100 μL and the temperature of the autosampler was set at 4 °C. For speciation and total analysis, the lens parameters were optimised with a solution of 1 μg L^{-1} of Ga, Y, Tl and Ce. Hydrogen was used in the reaction cell at 3.5 mL min^{-1}. To remove potential interferences during Se measurement, a solution of 10 μg L^{-1} of Ge was added and used as an internal standard to correct any plasma fluctuation. Isotopes ^{72}Ge, ^{77}Se, ^{78}Se, ^{125}Te and ^{126}Te were monitored. Standards were used for external calibration and quantification. Stock solution (VWR) was used for the total concentration analysis and sodium selenite (Alpha Aesar), sodium selenate (Alpha Aesar), sodium tellurite (Alpha Aesar) and telluric acid (Sigma Aldrich) were used for speciation. The elemental forms of Se were prepared as described by Aborode et al. (2015) and obtained as $SeSO_3$.

5. Results

5.1. Sample descriptions

The Kisgruva site is characterised by sporadic exposures of previously worked sulphide ore and metamorphic bedrock. Former workings also host standing pools of orange-yellow and clear water. Water extracted from sulphide ore and weathered ore crust samples show a pH of 4.0 and 2.2 respectively. Sulphide ore lenses are typically < 1 m thick. The metamorphic bedrock contains a high abundance of quartz (~40% of modal mineralogy), plagioclase (~30%), biotite (~10%), chlorite (~5%), hornblende (~5%) and amphibole (~5%). Pyrite is evident as sporadic and disseminated phases in the metamorphic bedrock.

In sulphide ore samples, the abundant sulphide-rich zones contain a mixture of chalcopyrite and (predominantly) pyrite, though pyrrhotite has also been previously identified in the region (NGU, 2017; Kotková et al., 2018). Bands of biotite are common, which exhibit a clear

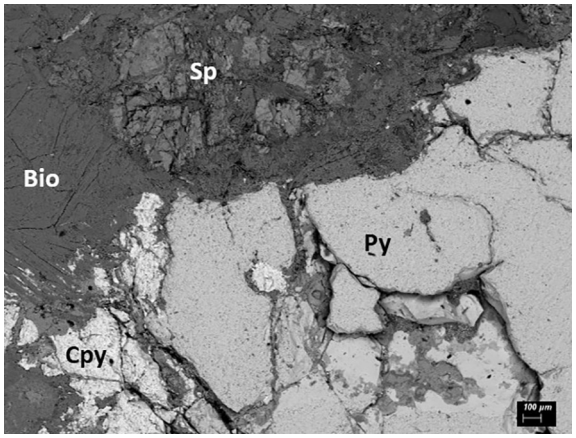

Fig. 3. SEM backscatter image of Kisgruva sulphide ore. Py = pyrite; Cpy = chalcopyrite; Bio = biotite; Sp = Zn spinel.

metamorphic fabric (alignment of micas to crenulated fabric). Fracturing is present throughout sample (0.1–0.5 mm), particularly in the more competent sulphidic zones. Fractures within biotite zones are filled predominantly with chlorite. Fractures and veins within sulphide zones are filled with goethite and jarosite, as well as chlorite and quartz. The Kisgruva sulphide ore is predominantly composed of pyrite, with pyrrhotite, chalcopyrite, gahnite (Al-Zn spinel), amphibole and biotite also evident (Fig. 3).

The sulphide ore contains abundant selenides (predominantly clausthalite (PbSe), with minor naumannite (Ag_2Se); Fig. 4), and tellurides (predominantly hessite (Ag_2Te), with minor altaite (PbTe) and tellurobismuthite (Bi_2Te_3); Fig. 5). Clausthalite phases identified in the sulphide ore samples typically show a small degree of alteration, with Te replacing Se and forming small amounts of altaite. In some instances, clausthalite forms a rim around hessite inclusions (Fig. 6). Inclusions of clausthalite, hessite, naumannite, altaite and tellurobismuthite are typically 5–25 μm in length and are common in pyrite (occurring less frequently in chalcopyrite). In general, the telluride and selenide phases are discreet (except for altaite with PbSe), but within close proximity to each other. Hessite phases generally contain more oxygen in the chemical structure than clausthalite. Inclusions of clausthalite and naumannite often occur in clusters, concentrated closely within larger pyrite and (less typically) chalcopyrite phases. Where mineralisation occurs within chalcopyrite, this is more commonly hessite, while clausthalite is the most abundant phase found within pyrite. Selenides and tellurides do not occur outside of the sulphide phases. Sulphide ore samples also contain disseminated phases of hessite within larger

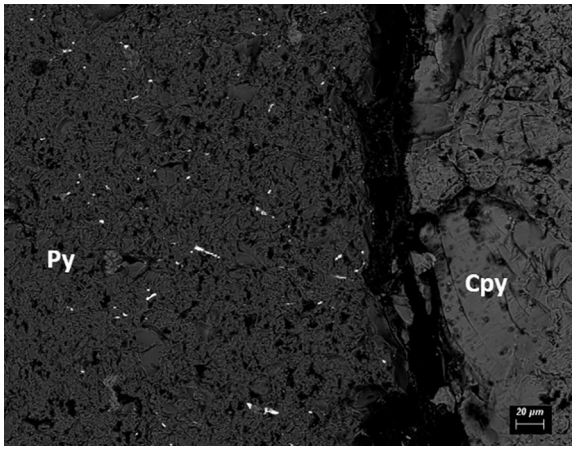

Fig. 4. SEM backscatter image of Kisgruva sulphide ore containing abundant Ag and Pb selenides (bright coloured inclusions) concentrated in pyrite.

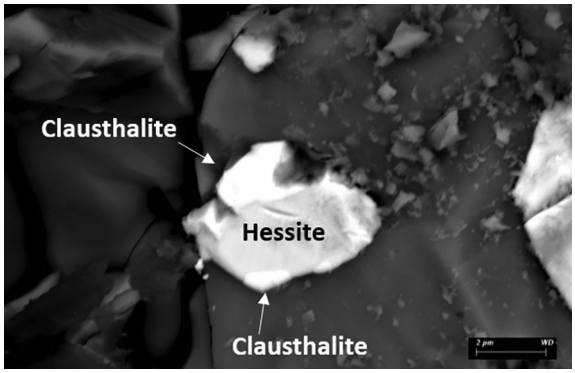

Fig. 5. SEM backscatter image of a sulphide ore containing an Ag telluride with an outer Pb selenide rim.

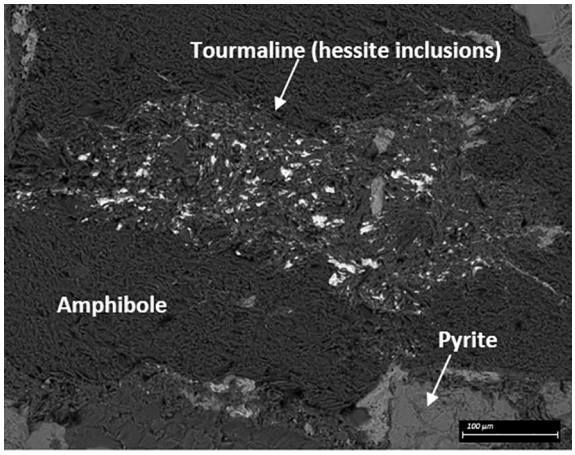

Fig. 6. SEM backscatter image of a telluride-bearing tourmaline crystal within the sulphide ore.

tourmaline phases (Fig. 6). The modal mineralogy of the sulphide ore samples is:

- Pyrite – 30%
- Biotite – 20%
- Chalcopyrite – 10%
- Gahnite – 10%
- Quartz – 7%
- Chlorite – 5%
- Jarosite – 5%
- Goethite – < 5%
- Sphalerite – < 5%
- Selenides – < 1%
- Tellurides – < 1%

Sulphide ore exposures are typically weathered across the site, showing crumbling crusts of loose orange rock (individual pieces of < 2 cm in length) on the outer surface of the outcrops (referred to here as “weathered ore crust”). Individual mineral phases are not discernible by SEM in weathered ore crust samples, though XRD analysis indicates the presence of chlorite (14.0 Å, 7.1 Å, 4.7 Å and 2.8 Å), goethite (4.6 Å and 3.0 Å), jarosite (5.1 Å, 3.1 Å and 1.4 Å), pyrite (3.3 Å, 2.2 Å and 1.6 Å), chalcopyrite (3.0 Å and 2.6 Å), haematite (5.0 Å), marcasite (3.4 Å) and minor quartz (3.4 Å) (Fig. 7).

5.2. Whole rock geochemistry

Whole rock geochemical results are shown in Table 2. Across sample types, Se correlates positively with Te (Fig. 8), and Se and Te have a

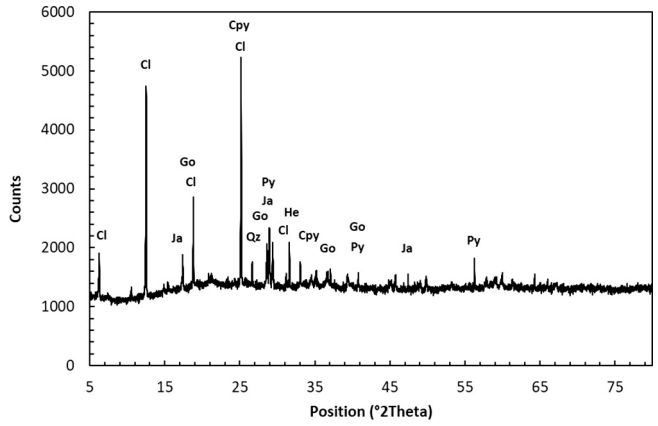

Fig. 7. XRD spectra and notable peaks showing main mineral phases in weathered ore crust deposits. Cl = chlorite; Ja = jarosite; Go = goethite; Cpy = chalcopyrite; Ma = marcasite; Qz = quartz; Py = pyrite; He = haematite.

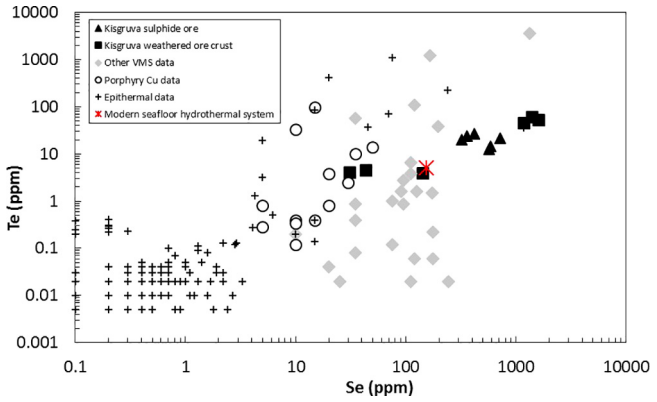

Fig. 8. Cross plot of Se vs. Te for Kisgruva sulphide ore and weathered ore crust. Volcanogenic massive sulphide (VMS), porphyry, epithermal and modern seafloor hydrothermal data also shown for comparison (Auclair et al., 1987; Hannington et al., 2004; Vikentev et al., 2004; Ishihara and Endo, 2005; Layton-Matthews et al., 2005; TH Cresgate, 2016; Vikentev, 2016; Bullock et al., 2017; OSNACA, 2018).

positive correlation with S and TOC (Fig. 9), as well as Ag, Au, As and Co. The sulphide ore contains ~0.05% organic matter, while the weathered ore crust contains ~0.34% TOC.

5.2.1. Metamorphic bedrock

Metamorphic bedrock samples generally contain lower average and maximum trace element contents compared to sulphide ore and weathered ore crust samples. Samples are enriched in Se and Te compared to crustal averages (mean crustal composition: Se = 0.04 ppm and Te = 2 μg kg^{-1}; Rudnick and Gao, 2014), with Se 10 ppm to 73 ppm and Te 0.4 ppm to 1.1 ppm (Table 2). There was no detectable Au in the metamorphic bedrock samples, with trace TOC (average 0.005%).

5.2.2. Sulphide ore

Sulphide ore samples show enrichment of Se and Te typically higher than comparable sulphide ore deposits from other studies, such as volcanogenic massive sulphide (VMS), porphyry and epithermal deposits (Fig. 10). Sulphide ores contain Se of 320 ppm to 718 ppm, and Te of 12 ppm to 27 ppm (Table 2). Samples are also high in other chalcophile elements which show a chemical affinity to Se and Te, such as S (up to 38.1%), Ag (6–17 ppm), Au (0.1–0.2 ppm), As (up to 303 ppm), Co (up to 143 ppm), Cu (2–2.4%), Mn (up to 749 ppm), Pb (up to 662 ppm) and Zn (2–2.4%). Sulphide ore samples show the highest Cu, Hg, Mn, Pb, S and Zn across all sample types. Sulphide ore samples contain an average of 0.05% TOC.

5.2.3. Weathered ore crust

Weathered ore crust samples are highly variable in trace element concentrations, generally showing higher Se and Te content than the sulphide ore and metamorphic bedrock samples (Table 2). Weathered ore crust samples are also higher in maximum Ag, As, Au, Co, Fe and TOC (0.6%) content. Samples contain 31 ppm to 1590 ppm Se and 3.9 ppm to 62 ppm Te. Samples contain ore grade Cu (1.3%), as well as high Au (0.5 ppm) and Ag (42 ppm). Weathered ore crust samples contain lower S (average 5.2%) than the sulphide ore (average 25.6%).

5.3. Mineral geochemistry

Previous studies have shown that Se and Te can concentrate in pyrite, substituting for S (Huston et al., 1995; Chouinard et al., 2005;

Table 2
Mineral (LA-ICP-MS) and whole rock (ICP-MS) geochemistry of Kisgruva sample types.

	Ag ppm	As ppm	Au ppm	Co ppm	Cu ppm or (%)	Fe %	Hg ppm	Mn ppm	Pb ppm	S %	Se ppm	Te ppm	Zn ppm or (%)	TOC (%)
Mineral														
Pyrite	62.2	376.4	0.1	–	2124	63.3	1.4	–	189.4	–	687.6	80.9	–	–
Pyrite	26.1	408.1	0.2	–	476	39.0	0.4	–	1274	–	644.7	49.5	–	–
Pyrite	156.7	288.8	0.1	–	3803	26.7	0.5	–	271.3	–	293.9	78.8	–	–
Whole rock														
Sulphide ore	17.2	278	0.11	141.0	(2.1)	28.5	1.6	441	662.0	36.6	718.3	21.8	(2.4)	0.016
Sulphide ore	11.3	163.5	0.13	73.5	8260	27.7	0.9	749	127.5	12.2	590.0	14.4	6870	0.141
Sulphide ore	12.5	219	0.18	142.5	9760	26.1	5.0	276	85.6	24.7	570.0	12.7	(2.2)	0.002
Sulphide ore	6.1	303	0.15	75.9	3140	25.5	6.1	258	105.5	27.4	360.0	23.7	(2.0)	0.003
Sulphide ore	16.9	267	0.09	142.0	(2.4)	19.9	0.3	237	43.0	14.3	320.0	19.7	934	0.043
Sulphide ore	12.6	280	0.02	145.5	7410	28.1	2.7	151	85.5	38.1	420.0	27.1	7720	0.126
Metamorphic bedrock	0.2	123	< 0.02	36.7	89	7.3	0.2	104	25.7	5.7	73.1	0.4	258	0.001
Metamorphic bedrock	0.9	110	< 0.02	37.9	200	5.4	0.2	87	69.3	6.1	25.8	1.1	129	0.016
Metamorphic bedrock	0.7	27.6	< 0.02	42.6	699	5.5	0.1	97	7.7	5.1	10.7	0.7	64	0.002
Metamorphic bedrock	0.8	111	< 0.02	39.2	177	4.9	0.1	6.0	64.6	6.4	26.0	0.8	15	0.001
Weathered ore crust	41.9	332	0.52	199.5	(1.3)	22.1	0.8	306	76.3	8.6	1402	62.1	580	0.338
Weathered ore crust	4.1	65.7	0.04	24.9	2810	29.1	0.5	497	49.2	3.9	141.0	3.9	1270	0.603
Weathered ore crust	0.6	35.3	< 0.02	33.1	142	3.7	0.3	258	67.1	1.2	31.0	4.1	570	0.038
Weathered ore crust	1.3	48.4	0.03	80.4	766	5.9	0.1	107	63.9	3.1	43.1	4.5	70	0.523
Weathered ore crust	39.9	357	0.44	256	(1.7)	25.2	0.8	354	75.1	8.6	1590	53.6	624	0.338
Weathered ore crust	42.1	360	0.48	227	(1.5)	24.2	0.8	303	78.3	5.8	1179	46.3	581	0.383

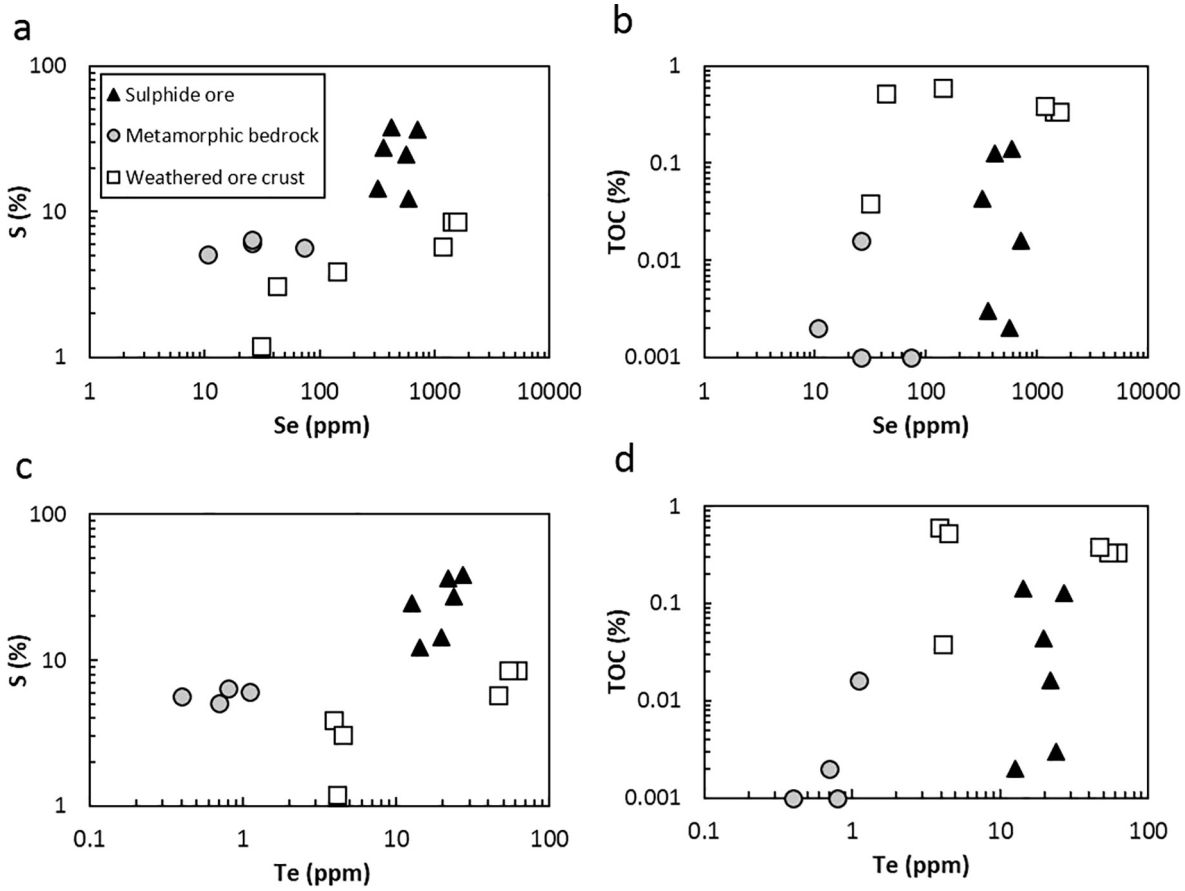

Fig. 9. Cross plots of (a) S (%) vs. Se (ppm), (b) TOC (%) vs. Se, (c) S vs. Te (ppm) and (d) TOC vs. Te.

Kesler et al., 2007; Keith et al., 2017), or concentrate within selenide (Se^{2-}) and telluride (Te^{2-}) inclusions (Emsbo et al., 2003; Pals et al., 2003; Cook et al., 2009a; Tanner et al., 2016; Keith et al., 2017). Analysis of predominantly inclusion-free pyrite phases within the sulphide ore reveals high concentrations of Ag (26–157 ppm), As (289–409 ppm), Se (294–688 ppm) and Te (49–81 ppm) (Table 2 and Fig. 10). Laser ablation maps show that As, Cu, Se and, to a lesser extent, Te, are generally high throughout the pyrite phases (Fig. 10). For As, Se and Te, concentrations are higher towards the edges of the pyrite. As well as a high content throughout pyrite, Se and Te also show disseminated areas of high concentrations, in some instances, up to 10,000 ppm and 1000 ppm respectively. Though the selected pyrite crystals are generally inclusion-free, these Se and Te hotspots may correspond to micron-sized Se^{2-} and Te^{2-}, which concentrate towards the edges of some pyrites (as evident in SEM imagery; Figs. 4 and 10). Other elements, such as Ag, Au, Hg and Pb, predominantly show concentrated and disseminated phases of high content within pyrite (Fig. 10).

5.4. Se and Te speciation

Both selenite (SeO_3^{2-}) and tellurite ion species were identified in weathered ore crust samples by phosphate and sodium hydroxide extraction methods (Fig. 11), but no elemental forms (Se^0 and Te^0) nor selenate (Se(VI))/tellurate (Te(VI)) were detected. Of the extractable Se (~74.2% of total Se), only 7% concentrates on oxide minerals, with 93% adsorbed to organic matter (Se(-II)). For extracted Te (~11%), ~15% is adsorbed to oxide minerals, and ~85% adsorbed to organic matter (Te(-II)).

6. Discussion

6.1. Weathered ore crust development

The main mineral phases present in the weathered ore crust include chlorite, goethite, jarosite, pyrite, chalcopyrite, haematite, marcasite and quartz (Fig. 7). These minerals resulted from acidic weathering and oxidation of mineral phases from the primary sulphide ore and/or the crystalline metamorphic bedrock, either as alteration products or remnant impurities. Oxidation of phases such as hessite within the sulphide ore indicates weathering within the rock has taken place. Phases such as quartz and chlorite in the weathered ore crust represent remnant impurities from the sulphide ore and metamorphic bedrock, which are often high in quartz and chlorite. Additional chlorite may have also resulted from weathering of biotite (high in sulphide ore and metamorphic bedrock) under acidic conditions. Some pyrite and chalcopyrite were also retained as impurities from the sulphide ore. However, pyrite is not very resistant to weathering when in contact with oxygen and an aqueous fluid, and will break down to produce sulphuric acid, sulphates and haematite. Sulphuric acid will be carried away in solution as acid mine drainage (evident at Kisgruva in standing pools of acidic waters), and haematite is evident at Kisgruva in the weathered ore crust. Weathering of pyrite also produces jarosite, ferric oxides (haematite) and hydroxides, such as goethite (Frau, 2000; Benvenuti et al., 2000; Lu et al., 2005), all of which are present in Kisgruva weathered ore crust samples. Pyrrhotite (previously reported in the Kongsberg region sulphide ores; NGU, 2017; Kotková et al., 2018) weathering can also produce secondary pyrite, jarosite, goethite and marcasite (Burns and Fisher, 1990; Bhatti et al., 1993), and hornblende (high in metamorphic bedrock) can also produce additional goethite (Velbel, 1989).

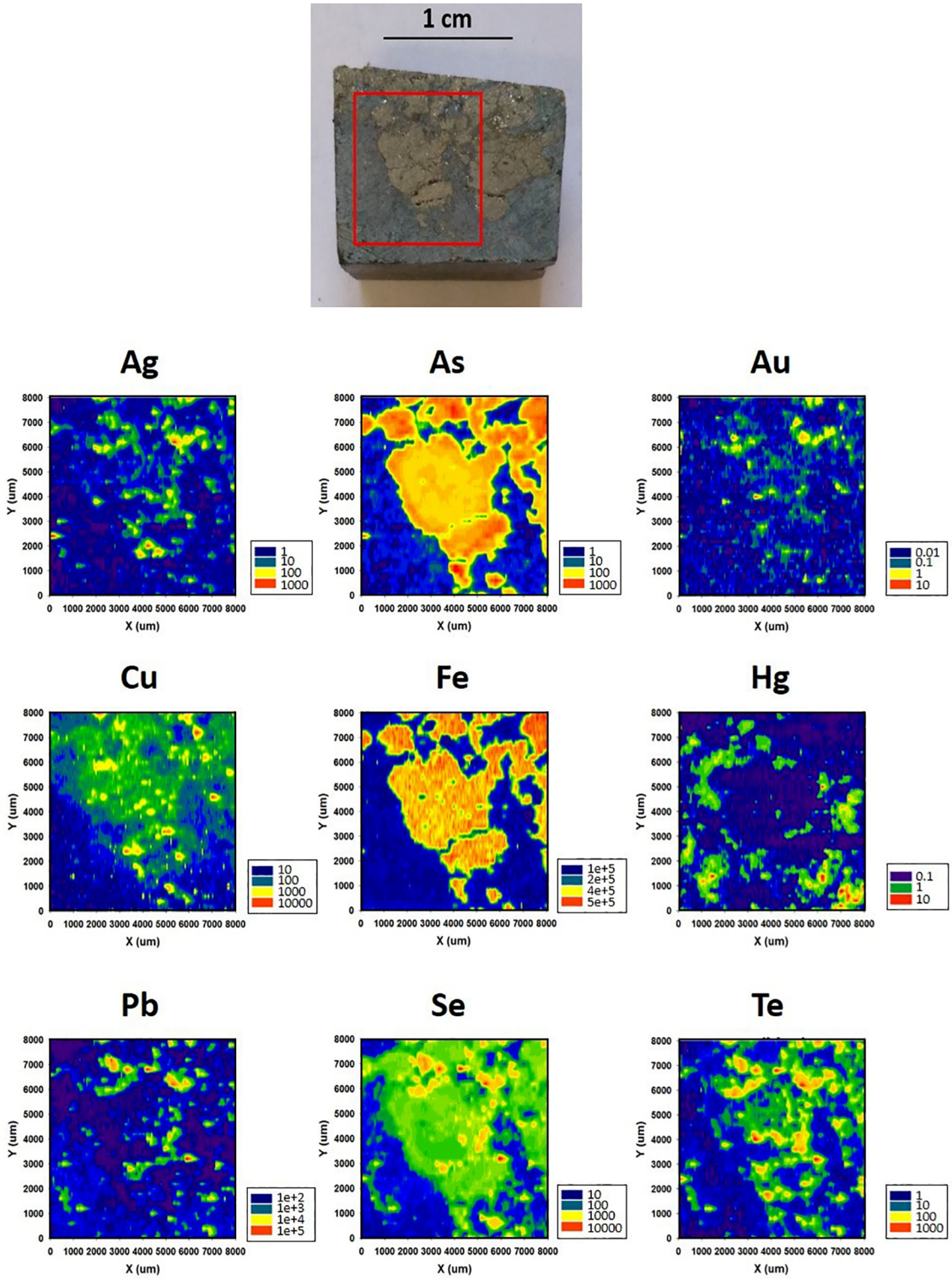

Fig. 10. LA-ICP-MS element maps of predominantly inclusion-free pyrite phases from Kisgruva sulphide ore samples (scale in ppm).

6.2. Se and Te residence

Inclusions of clausthalite, hessite, naumannite, altaite and tellurobismuthite (Figs. 4–6) within sulphide ore samples provide the dominant source of Se and Te in the Kisgruva sample suite. Elevated concentrations of Se and Te within in pyrite crystal structures from the ore (Fig. 10) are also contributing sources of elevated Se and Te in Kisgruva samples, as evident by the LA-ICP-MS maps of generally inclusion-free pyrites (Fig. 10). Pyrite and other sulphide phases in the primary ore (pyrrhotite, chalcopyrite, sphalerite and galena) also host other highly concentrated chalcophile elements such as As, Hg, Cu, Pb, Zn and Au. The low organic content of the sulphide ores (0.05%) suggests that the majority of Se and Te is held in clausthalite, hessite, minor selenide and telluride phases, and sulphide phases, and not sorbed on to organic matter. High Se and Te concentrations within weathered ore crust samples indicates that Se and Te were mobilised once the exposed ore was weathered at the surface (or in the sub-surface), and the host mineral phases decomposed.

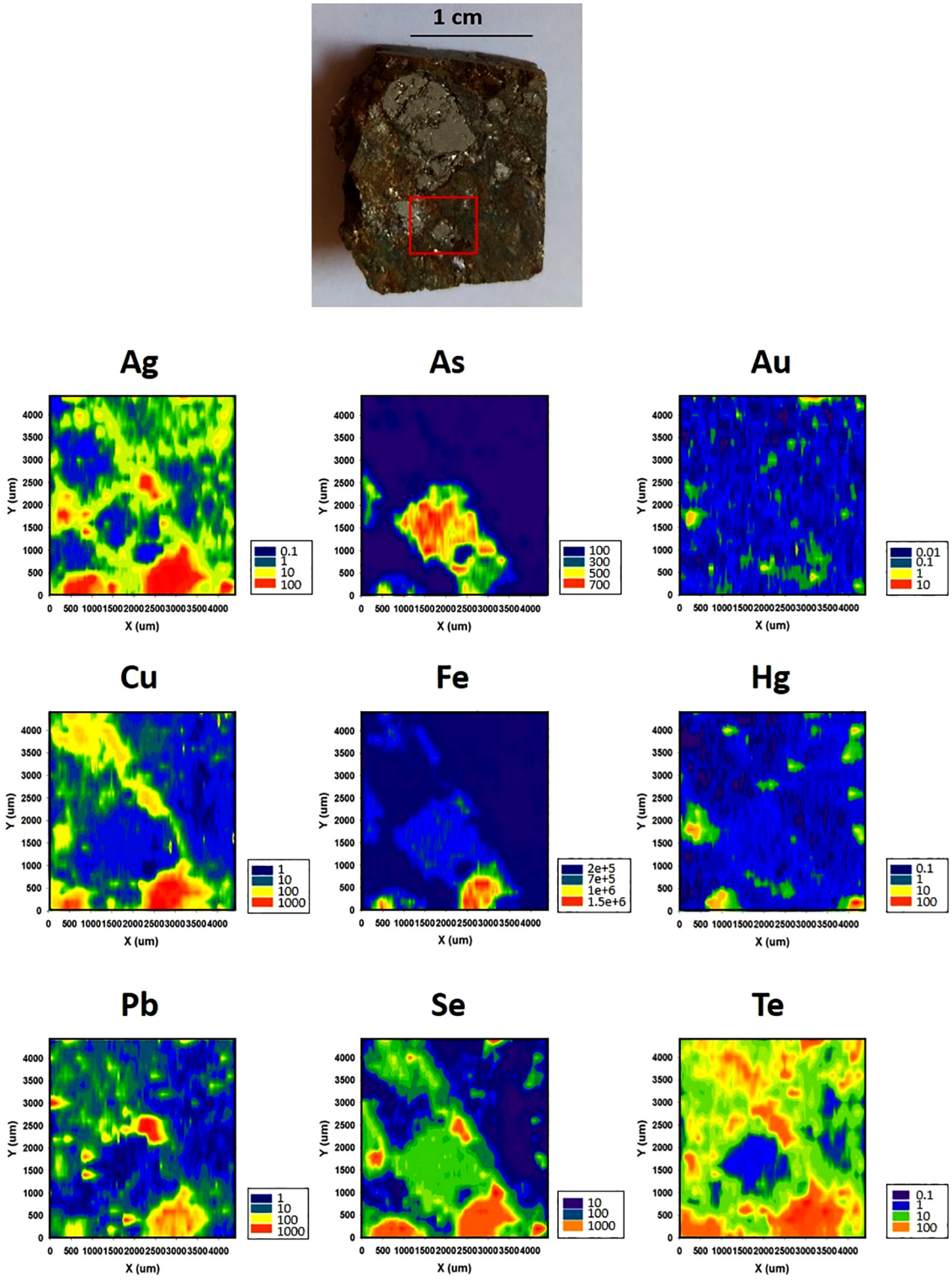

Fig. 10. (*continued*)

Phases of Se^{2-} and Te^{2-} have previously been shown to form in similar sulphide ore-producing settings, such as the Au-enriched VMS deposits of The Urals (Vikentev, 2006; Vikentev et al., 2006; Belogub et al., 2008; Maslennikova et al., 2008; Cook et al., 2009b). Tellurides occurring with common sulphides in such settings may form from recrystallisation of Au during late (low-temperature) hydrothermal processes and/or overprinting during greenschist facies metamorphism (Vikentev, 2006). This may be the case with Kisgruva (Au detected within sulphide ore samples), with a hydrothermal origin followed by later medium grade regional metamorphism. Sulphosalts and associated Se^{2-} and Te^{2-} may also concentrate by sulphidation and oxidation during interactions between the reduced hydrothermal fluids and the oxidised seawater, and associated microbial activity, as previously described at the Urals (Belogub et al., 2008; Maslennikova et al., 2008; Cook et al., 2009b).

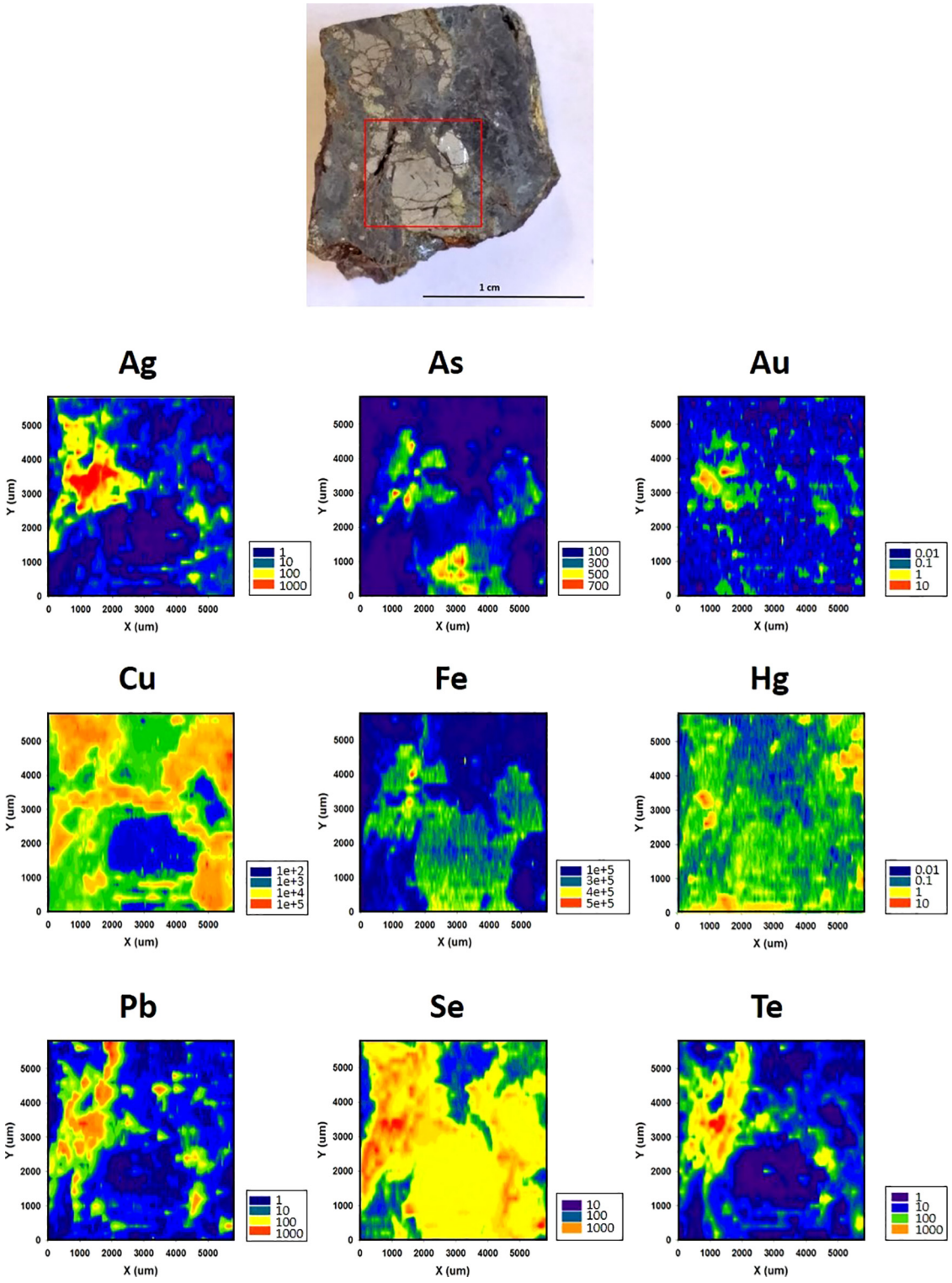

Fig. 10. (*continued*)

6.3. Se and Te mobilisation

Both Se and Te have a range of oxidation states (−II to +VI), with some species more mobile than others under changing redox conditions, mainly due to the adsorption processes of Fe oxides and clay minerals (Davidson, 1960; White and Dubrovsky, 1994; Kulp and Pratt, 2004). Inclusions of clausthalite, hessite, naumannite, altaite and tellurobismuthite, identified in Kisgruva sulphide ores, are easily decomposed under oxidising conditions, converting to SeO_3^{2-} and TeO_3^{2-} ions. Ions of SeO_3^{2-} and TeO_3^{2-} are also highly mobile (Davidson, 1960; Balistrieri and Chao, 1987), particularly under acidic conditions such as those identified at Kisgruva. The oxidised SeO_3^{2-} and TeO_3^{2-} ion species have been identified in weathered ore crust samples (Fig. 11), mobilised and forming from clausthalite, naumannite, tellurobismuthite and hessite from the sulphide ore. Soluble forms of Se and Te are adsorbed strongly onto Fe oxides (e.g. goethite, haematite) in acid conditions (Balistrieri and Chao, 1990, Manning et al., 1998, Su and Suarez 2000; Rovira et al., 2008), with SeO_3^{2-} ions absorbing to

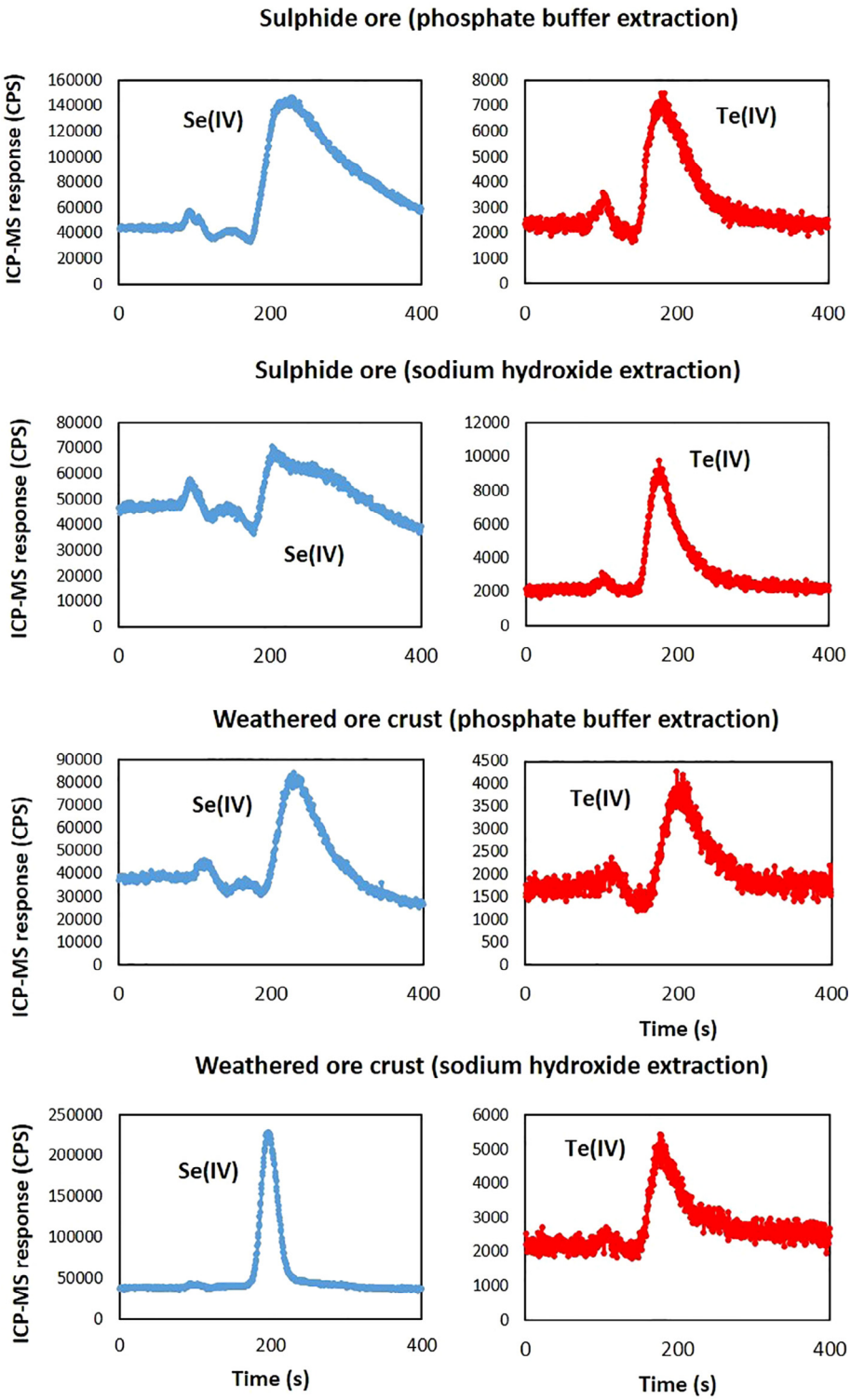

Fig. 11. Chromatographs of Se and Te speciation in weathered ore crust samples (selenite (SeO_3^{2-})) and tellurite (TeO_3^{2-}) ions) by phosphate buffer and sodium hydroxide extraction methods. Chromatographs show that SeO_3^{2-} and TeO_3^{2-} ions were the only detectable species.

jarosite (formed from oxidation of sulphides from the primary ore) at lower pH values. Selenate has a much lower affinity for Fe oxides than SeO_3^{2-} (Su and Suarez 2000), which may explain its absence in the weathered ore crust samples. Elemental Se and Te may still be present and remained unextracted during speciation experiments. For instance, in the case of Se, abiotic reduction of SeO_3^{2-} to Se^0 can occur in the presence of Fe oxides in deposits such as lake sediments (Chen et al., 2008; Maher et al., 2010).

A combination of fine particle size (typically colloidal) and the affinity of Fe oxides for Se and Te means that weathered ore crusts may provide a natural trap for percolating solutes (Fig. 12). The higher Se and Te concentrations in the weathered ore crust compared to the sulphide ore can be attributed to a higher organic content and the presence of goethite, haematite and jarosite. The majority of extractable Se and Te was bound to organic matter (reducing agent to immobilise Se and Te), with the rest adsorbed to jarosite and Fe oxides. Though

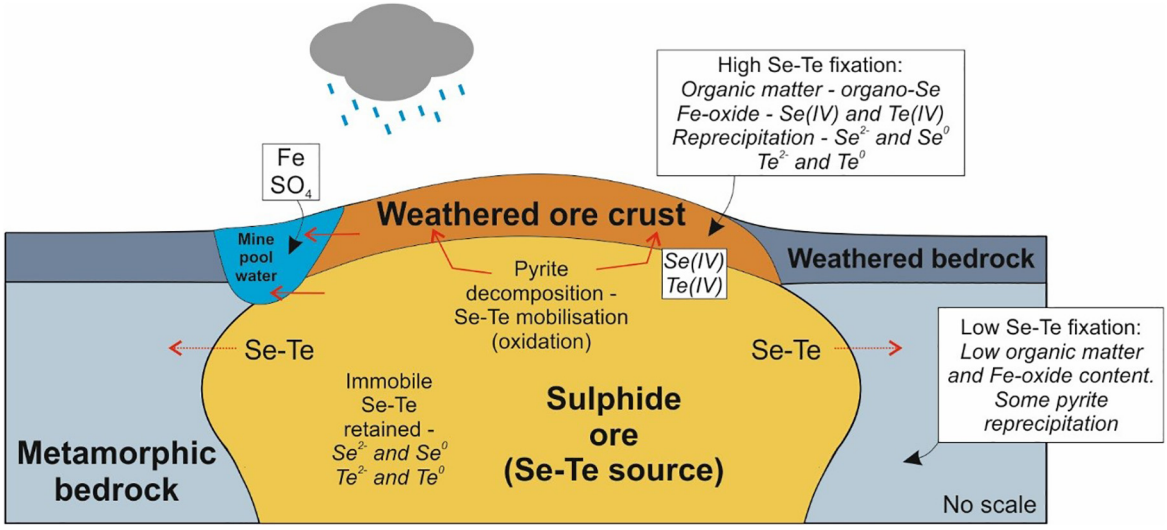

Fig. 12. Source, mobility and fixation of Se and Te species at the Kisgruva site.

pyrite was identified in the metamorphic bedrock, lower concentrations of Se and Te were identified, owing to the low organic matter (average of 0.005%) and Fe oxide content to act as a sink for these trace elements. Trace organic matter, such as that detected in the sulphide ore, may have accumulated by entrapment and thermal maturation of sedimentary organic matter by hydrothermal fluids during ore formation (Rasmussen and Buick, 2000). The organic matter in the weathered ore crust (average of 0.4%) may also be residual material from ore formation, with additional accumulation sunken from plants and regolith. Other carbon-rich material has been identified as coalblende-bearing aggregate silver samples from areas of Kongsberg to the north of Kisgruva (Kotková et al., 2018). The high amount of coalblende in these Kongsberg samples has been attributed to fluids derived from the Cambro-Silurian organic-rich black shales of the Oslo Graben (Kotková et al., 2018), which lie 2–3 km east of Kisgruva (Fig. 1). This suggests that carbon and other organic materials from these black shales may have been mobilised and transported through the Kisgruva region to the more northerly Kongsberg silver deposits and may therefore have supplied some additional organic material to the lithological units and weathered ore crust, though this is only speculated. The presence of organic matter, and associated microorganisms such as S- and Fe-oxidising bacteria, can increase the weathering, mobility and metal release from the ore (Leslie et al., 2015).

6.4. Economic considerations

Identification of high Se and Te in pyritic ores and associated weathered deposits is essential for future advances and decisions in ore processing and management of both former and active metalliferous mining sites. While Se and Te are not currently considered viable extractable primary resources (i.e. their current production is typically as by-product recovery, such as during Cu processing; Brown, 2000; Plant et al., 2013), their presence in high abundances may prove important as methods of critical element extraction continue to improve globally, as demand rises and worldwide conventional Se- and Te-hosting deposits are exhausted. Due to their high pyrite content and economic significance, a comparison between previously studied VMS, epithermal and porphyry deposits worldwide and the Kisgruva site can provide an indication on the potential suitability of Kisgruva as a site of economic importance (Fig. 8).

Kisgruva Se is equivalent to, or higher than, modern seafloor hydrothermal systems (~154 ppm Se; Hannington et al., 2004) and Cu-rich chimneys at seafloor hydrothermal black smoker sites (~1000 ppm Se; Auclair et al., 1987) (Fig. 4). Archived Se and Te data (available online) from 24 VMS localities worldwide contain an average of 88.5 ppm Se (maximum 245 ppm), and an average of 9.4 ppm Te (maximum 109 ppm) (OSNACA, 2018). Elsewhere worldwide, Se and Te are similar or higher than other notable VMS deposits, such as Shimokawa and Tsuchikura mines, Japan (330 ppm Se; Ishihara and Endo, 2005), Parys Mountain, UK (173 ppm Se and 1.5 ppm Te; Bullock et al., 2017) and Lagoa Salgada, Portugal (194 ppm Se; TH Cresgate, 2016). The Uchalinsk copper-zinc-pyritic district (the Urals) has been previously noted as one of the largest ore belts of massive sulphide reserves in the world and is also known to contain notably high Se and Te content (Vikentev, 2016). The highest grades from the Uchalinsk and Uzelginsk deposits, Russia, show concentrations of Te that are up to 3 magnitudes higher than Kisgruva (3650 ppm and 1239 ppm respectively; Vikentev et al., 2004; Vikentev, 2016). However, Se concentrations at Kisgruva are similar, and in some cases slightly higher (up to 1324 ppm Se at Uchalinsk ore district, and 154 ppm at the Uzelginsk deposit; Vikentev et al., 2004; Vikentev, 2016). Highly economic areas of Finlayson Lake district, Yukon, Canada, show higher Se (up to 3420 ppm) than Kisgruva, but Te is not measured (Layton-Matthews et al., 2005). Kisgruva samples are generally higher in Se than most previously determined porphyry and epithermal deposits (OSNACA, 2018), though some porphyry and epithermal deposits contain equivalent or higher Te (Fig. 8).

At present, Se and Te are not directly mined, and are typically sourced as a by-product from Cu or Ni production. Therefore, well-constrained cut-off grades are not considered for these elements. This means that some deposits that are rich in Se and Te are neither mined nor targeted at all, and are often deliberately avoided during mining. This is particularly true of Se, which is considered a contaminant in mining, such as at U mine-waste sites (Dahlkamp, 2010; Abzalov, 2012; Bullock and Parnell, 2017). However, with improved knowledge, expertise and more efficient processing, this may change, particularly with the growth of industries responsible for alloys, photovoltaic products and nanotechnologies (Jin et al., 2016; Wei et al., 2016). Meeting future demand requires new approaches, including a change from by-production to targeted processing of Se- and Te-rich materials. The future supply of a range of Se and Te may be resolved by the processing of mineral hosts, such as sulphides (Cline and Hofstra, 2000; Reich et al., 2013; Deditius et al., 2014; Keith et al., 2017). The growing necessity for sources of E-tech elements has led to an increasing focus on new potential worldwide sources of Se and Te, and a review of former base metal sites may form an important part of this shift. With a potential 581 thousand tons of reserves and 3200 m^3 volume of dump remaining, the Kisgruva site could hold potentially economic Se and Te

in both sulphide ore materials and weathered ore crust deposits. Based on these reserve estimations, and average grams per tonne Se and Te across sulphide ore and weathered ore crust measured in this study, the Kisgruva site may contain up to 367,000 kg Se and 130,560 kg Te in reserves, and a further 3340 kg Se and 130 kg in remaining dump.

7. Conclusions

The Kisgruva site contains exceptionally high concentrations of Se and Te within the sulphide ore and weathered ore crust deposits, relative to economic VMS, porphyry and epithermal deposits worldwide. High concentrations are sourced from sulphide minerals and disseminated clausthalite, hessite, and minor naumannite, altaite and tellurobismuthite phases within the sulphide ore, mobilised under oxidising conditions upon weathering of the exposed and sub-surface ore. The higher concentrations of the weathered ore crust deposits are attributed to high organic, goethite, haematite and jarosite contents, acting as a sink for Se and Te, fixing SeO_3^{2-} and TeO_3^{2-} ion species and Se and Te sorbed on to organic matter. Though high Se and Te concentrations may currently be considered a contaminant in base metal mining and production, the rising demand for these trace elements may highlight the need to identify and review sites such as Kisgruva to meet requirements, particularly with improved knowledge and means of efficient processing. Results have important implications for Se- and Te-bearing ores and weathered products as potential critical element resources, particularly as means of extraction continue to improve. While high Se and Te in selected sample areas do not necessarily apply to the full extent of the extractable ore body, the identification of enriched regions and deposits allows for the identification of specific targets and natural enrichment processes which may occur regionally or at similar deposits worldwide.

Acknowledgements

The authors are extremely grateful to Kåre Kullerud of the Norsk Bergverksmuseum (Kongsberg) for sharing his wealth of knowledge of the Kisgruva site and assisting in accessibility. The authors also wish to thank Abbie Mclaughlin (University of Aberdeen) for her assistance with XRD analysis. The authors thank the anonymous reviewers for their careful reading and corrections of the manuscript.

Funding

This work was supported by the UK Natural Environment Research Council (NERC); Minerals Security of Supply (SoS) Grant NE/M010953/1, Tellurium and Selenium Cycling and Supply (TeaSe).

References

Aborode, F.A., Raab, A., Foster, S., Lombi, E., Maher, W., Krupp, E.M., Feldmann, J., 2015. Selenopeptides and elemental selenium in Thunbergia alata after exposure to selenite: quantification method for elemental selenium. Metallomics 7, 1049–1198.
Abzalov, M.Z., 2012. Sandstone-hosted uranium deposits amenable for exploitation by in situ leaching technologies. Appl. Earth Sci. 121 (2), 55–64 Transactions of the Institution of Mining and Metallurgy, Section B.
Andersen, T., Griffin, W.L., Jackson, S.E., Knudsen, T.-L., Pearson, N.J., 2004. Mid-Proterozoic magmatic arc evolution at the southwest margin of the Baltic shield. Lithos 73, 289–318.
Anthony, J.W., Bideaux, R.A., Bladh, K.W., Nichols, M.C., 1990. Handbook of Mineralogy. Mineralogical Society of America, Chantilly, VA 20151-1110, USA.
Auclair, G., Fouquet, Y., Bohn, M., 1987. Distribution of selenium in high-temperature hydrothermal sulfide deposits at 13 degrees North, East Pacific Rise. Can. Mineral. 25, 577–587.
Ba, L.A., Döring, M., Jamier, V., Jacob, C., 2010. Tellurium: an element with great biological potency and potential. Org. Biomol. Chem. 8, 4203–4216.
Balistrieri, L.S., Chao, T.T., 1987. Selenium adsorption by goethite. Soil Sci. Soc. Am. J. 51, 1145–1151.
Balistrieri, L.S., Chao, T.T., 1990. Adsorption of selenium by amorphous iron oxyhydroxide and manganese dioxide. Geochim. Cosmochim. Acta 54, 739–751.
Bancroft, P., Nordrum, F.S., Lyckberg, P., 2001. Kongsberg revisited. Mineral. Rec. 32 (3), 181–205.
Belogub, E.E., Novoselov, K.A., Yakovleva, V.A., Spiro, B., 2008. Supergene sulphides and related minerals in the supergene profiles of VHMS deposits from the South Urals. Ore Geol. Rev. 33, 239–254.
Belzile, N., Chen, Y.W., 2015. Tellurium in the environment: a critical review focused on natural waters, soils, sediments and airborne particles. Appl. Geochem. 63, 83–92.
Benvenuti, M., Mascaro, I., Corsini, F., Ferrari, M., Lattanzi, P., Parrini, P., Costagliola, P., Tanelli, G., 2000. Environmental mineralogy and geochemistry of waste dumps at the Pb (Zn)-Ag Bottino mine, Apuane Alps, Italy. Eur. J. Mineral. 12, 441–453.
Bhatti, T.M., Bigham, J.M., Carlson, L., Tuovinen, O.H., 1993. Mineral products of pyrrhotite oxidation by Thiobacillus ferrooxidans. Appl. Environ. Microbiol. 59 (6), 1984–1990.
Bingen, B., Davis, W.J., Hamilton, M.A., Engvik, A., Stein, H.J., Skår, Ø., Nordgulen, Ø., 2008a. Geochronology of high-grade metamorphism in the Sveconorwegian belt, S. Norway: U-Pb, Th-Pb and Re-Os data. Norw. J. Geol. 88, 13–42.
Bingen, B., Nordgulen, Ø., Viola, G., 2008b. A four-phase model for the Sveconorwegian orogeny, SW Scandinavia. Norw. J. Geol. 88, 43–72.
Bjerkgård, T., 2012. N008 Kongsberg Ag. In: Eilu, P. (Ed.), Mineral Deposits and Metallogeny of Fennoscandia. Geological Survey of Finland, Special Paper 53, pp. 56–59.
Bjerkgård, T., 2015. Massive sulfides in Norway. NGU Focus Nr. 2, Feburary 2015.
Boyle, R.W., 1968. Fahlbands, sulfide schists, and ore deposition. Econ. Geol. 63, 835–840.
Bragg, W.H., 1912. X-rays and crystals. Nature 90, 219. https://doi.org.10.1038/090219a0.
Brown, R.D., 2000. Selenium and tellurium. In: U.S. Geological Survey Minerals Yearbook, U.S. Geological Survey, Reston, VA, USA, pp. 1–8.
Bugge, A., 1917. Kongsbergfeltets geologi. Nor. Geol. Unders. 82.
Bugge, A., 1928. Enforkastning i det syd-norske grunnfjell. Norges Geologiske Undersokelse Bull. 130, 1–124.
Bugge, A., 1937. Flesberg og Eiker. NGU Bull. 143, 118 pp.
Bullock, L.A., Parnell, J., 2017. Selenium and molybdenum enrichment in uranium roll-front deposits of Wyoming and Colorado, USA. J. Geochem. Explor. 180, 101–112.
Bullock, L.A., Parnell, J., Perez, M., Feldmann, J., Armstrong, J.G., 2017. Selenium and other trace element mobility in waste products and weathered sediments at Parys mountain copper mine, Anglesey, UK. Minerals 7 (11), 229.
Burns, R.G., Fisher, D.S., 1990. Iron-sulfur mineralogy of Mars' magmatic evolution and chemical weathering products. J. Geophys. Res. 95 (B9), 14415–14421.
Charykova, M.V., Krivovichev, V.G., 2017. Mineral systems and the thermodynamics of selenites and selenates in the oxidation zone of sulfide ores – a review. Mineral. Petrol. 111, 121–134.
Chen, Y.W., Truong, H.Y.T., Belzile, N., 2008. Abiotic formation of elemental selenium and role of iron oxide surfaces. Chemosphere 74, 1079–1084.
Chouinard, A., Paquette, J., William-Jones, A.E., 2005. Crystallographic controls on trace-element incorporation in auriferous pyrite from Pascua epithermal high sulfidation deposit: Chile-Argentina. Can. Mineral. 43, 951–963.
Cline, J.S., Hofstra, A.A., 2000. Ore-fluid evolution at the Getchell Carlin-type gold deposit, Nevada, USA. Eur. J. Mineral. 12, 195–212.
Cook, N.J., Ciobanu, C.L., Mao, J., 2009a. Textural control on gold distribution in As free pyrite from the Dongping, Huangtuliang and Hougou gold deposits, North China Craton (Hebei Province, China). Chem. Geol. 264, 101–121.
Cook, N.J., Ciobanu, C.L., Spry, P.G., Voudouris, P., the participants of IGCP-486, 2009b. Understanding gold-(silver)-telluride-(selenide) mineral deposits. Episodes 32, no. 4.
Dahlkamp, F.J., 2010. Geology of the uranium deposits. In: Uranium Deposits of the World, vol. 2. Springer, Verlag publisher, USA and Latin America, p. 517.
Davidson, D.F., 1960. Selenium in some epithermal deposits of antimony, mercury and silver and gold. U.S. Geol. Surv. Bull. 1112-A, 1–17.
Deditius, A.P., Reich, M., Kesler, S.E., Utsunomiya, S., Chryssoulis, S.L., Walshe, J., Ewing, R.C., 2014. The coupled geochemistry of Au and As in pyrite from hydrothermal ore deposits. Geochim. Cosmochim. Acta 140, 644–670.
Di Tullo, P., Pannier, F., Thiry, Y., Le Hécho, I., Bueno, M., 2016. Field study of time-dependent selenium partitioning in soils using isotopically enriched stable selenite tracer. Sci. Total Environ. 562, 280–288.
Downs, R.T., Hall-Wallace, M., 2003. The American mineralogist crystal structure database. Am. Mineral. 88, 247–250.
El-Shahawi, M.S., Al-Saidi, H.M., Al-Harbi, E.A., Bashammakh, A.S., Alsibbai, A.A., 2013. Speciation and determination of tellurium in water, soil, sediment and other environmental samples. In: Bakirdere, S. (Ed.), Speciation Studies in Soil, Sediment and Environmental Samples. CRC Press, Taylor & Francis Group, Boca Raton, pp. 527–544.
Emsbo, P., Hofstra, A.H., Lauha, E.A., Griffin, G.L., Hutchinson, R.W., John, D.A., Theodore, T.G., 2003. Origin of high- grade gold ore, source of ore fluid components, and genesis of the Meikle and neighboring Carlin-type deposits, northern Carlin Trend, Nevada. Econ. Geol. Spec. Publ. 98, 1069–1105.
Frau, F., 2000. The formation-dissolution cycle of melanterite at the abandoned pyrite mine of Genna Luas in Sardinia, Italy: environmental implications. Mineral. Mag. 64, 995–1006.
Gammon, J.B., 1964. A Geological Investigation of the Cobalt-fahlbands of the Modum Area, Norway. Unpub. Ph.D.. Thesis, Univ. of Durham, England.
Gammon, J.B., 1966. Fahlbands in the Precambrian of southern Norway. Econ. Geol. 61 (1), 174–188.
Hannington, M.D., Petersen, S., Herzig, P.M., Jonasson, I.R., 2004. A global database of seafloor hydrothermal systems, including a digital database of geochemical analyses of seafloor polymetallic sulfides. Geological Survey of Canada, Open File 4598. 1 CD-ROM.
A. Helland, A., 1879. Om forekomsten av Kobalt og Nikkelerster i Norge. Arkiv.f . Matem. og. Naturv. Bd. 4.

Howard, J.H., 1977. Geochemistry of selenium: formation of ferroselite and selenium behavior in the vicinity of oxidizing sulfide and uranium deposits. Geochim. Cosmochim. Acta 41, 1665–1678.
Huston, D.L., Sie, S.H., Suter, G.F., Cooke, D.R., Both, R.A., 1995. Trace elements in sulfide minerals from eastern Australian volcanic-hosted massive sulfide deposits; Part I, Proton microprobe analyses of pyrite, chalcopyrite, and sphalerite, and Part II, Selenium levels in pyrite; comparison with delta 34 S values and implications for the source of sulfur in volcanogenic hydrothermal systems. Econ. Geol. 90, 1167–1196.
Ishihara, S., Endo, Y., 2005. Indium and other trace elements in volcanogenic massive sulfide ores from the Kuroko, Besshi and other types in Japan. Bull. Geol. Surv. Japan 58 (1/2), 7–22.
Jin, R., Zhao, K., Pu, X., Zhang, M., Cai, F., Yang, X., Kin, H., Zhao, Y., 2016. Structural and photovoltaic properties of $FeSe_2$ films prepared by radio frequency magnetron sputtering. Mater. Lett. 179, 179–181.
Keith, M., Smith, D.J., Jenkin, G.R.T., Holwell, D.A., Dye, M.D., 2017. A review of Te and Se systematics in hydrothermal pyrite from precious metal deposits: insights into ore-forming processes. Ore Geol. Rev. 96, 269–282.
Kesler, S.E., Deditius, A.P., Chryssoulis, S., 2007. Geochemistry of Se and Te in arsenian pyrite: new evidence for the role of Se and Te hydrothermal complexes in Carlin and epithermal-type deposits. In: Kojonen, K.K., Cook, N.J., Ojala, V.J. (Eds.), Au–Ag–Te–Se Deposits, Proceedings of the 2007 Field Workshop (Espoo, Finland, August 26–31, 2007). Geological Survey of Finland 53, pp. 85–95.
Khamkhash, A., Srivastava, V., Ghosh, T., Akdogan, G., Ganguli, R., Aggarwal, S., 2017. Mining-related selenium contamination in Alaska, and the state of current knowledge. Minerals 7 (46). https://doi.org/10.3390/min7030046.
Kjerulf, T., Dahll, T., 1861. Om Kongsbergs Ertdistrikt. Nyt Magazin for Naturvidenskabene 11, 173–207.
Kotková, J., Kullerud, K., Šrein, V., Drábek, M., Škoda, R., 2018. The Kongsberg silver deposits, Norway: Ag-Hg-Sb mineralization and constraints for the formation of the deposits. https://doi.org/10.1007/s00126-017-0757-1.
Kulp, T.R., Pratt, L.M., 2004. Speciation and weathering of selenium in Upper Cretaceous chalk and shale from South Dakota and Wyoming, USA. Geochim. Cosmochim. Acta 68 (18), 3687–3701.
Lafuente, B., Downs, R.T., Yang, H., Stone, N., 2015. The power of databases: the RRUFF project. In: Armbruster, T., Danisi, R.M. (Eds.), Highlights in Mineralogical Crystallography. W. De Gruyter, Berlin, Germany, pp. 1–30 https://doi.org.10.1515/9783110417104-003.
Layton-Matthews, D., Scott, S.D., Peter, J.M., Leybourne, M.I., 2005. Transport and deposition of selenium in felsic volcanic-hosted massive sulfide deposits of the Finlayson Lake District, Yukon Territory, Canada. Mineral Deposit Research: Meeting the Global Challenge, pp. 643–646.
Lemly, A.D., 2004. Aquatic selenium pollution is a global environmental safety issue. Ecotoxicol. Environ. Saf. 59, 44–56.
Leslie, K., Sturm, A., Stotler, R., Oates, C.J., Kyser, K., Fowle, D.A., 2015. Marinobacter bacteria associated with a massive sulphide ore deposit affect metal mobility in the deep subsurface. Geochemistry 15, 319–326.
Lu, L., Wang, R., Chen, F., Xue, J., Zhang, P., Lu, J., 2005. Element mobility during pyrite weathering: implications for acid and heavy metal pollution at mining-impacted sites. Environ. Geol. 49, 82–89.
Maher, B., Roach, T., Doblin, M., Fan, T., Foster, S., Garrett, R., Möller, G., Oram, L., Wallschlager, D., 2010. Environmental sources, speciation and partitioning of selenium. In: Chapman, P.M., Adams, W.J., Brooks, M., Delos, C.G., Luoma, S.N., Maher, W.A., Ohlendorf, H.M., Presser, T.S., Shaw, P. (Eds.), Ecological Assessment of Selenium in the Aquatic Environment, first ed. Taylor & Francis, United States, pp. 47–92.
Maslennikova, S., Maslennikov, V., Herrington, R., 2008. Tellurium-bearing mineralization in Paleozoic black smokers. Abstract, 33rd International Geological Congress.
Manning, B.A., Fendorf, S.E., Goldberg, S., 1998. Surface structures and stability of arsenic (III) on goethite: spectroscopic evidence for inner-sphere complexes. Environ. Sci. Technol. 32, 2383–2388.
Min, M., Xu, H., Chen, J., Fayek, M., 2005. Evidence of uranium biomineralization in sandstone-hosted roll-front uranium deposits, northwestern China. Ore Geol. Rev. 26, 198–206.
Norges Geologiske Undersøkelse (NGU), 1981. Diamantboring ved Kisgruva. NGU Report 1650/7B.
Norges Geologiske Undersøkelse (NGU), 2017. The ore database. Deposit Area 604 – 050. Name of Deposit Area: Kisgruva. Available online: http://aps.ngu.no/pls/oradb/minres_deposit_fakta.Main?p_objid=6096&p_spraak=E.
Norsk Institutt For Vannforskning (NIVA), 2003. Avrenning fra Kongsberg Sølvverk. NIVA Report 4660-2003.
Northrop, H.R., Goldhaber, M.B., 1990. Genesis of the tabular-type vanadium–uranium deposits of the Henry Basin, Utah. Econ. Geol. 85, 215–269.
Ore Samples Normalised to Average Crustal Abundance (OSNACA), 2018. Brauhart et al. University of Western Australia, http://www.cet.edu.au/research-projects/special-projects/projects/osnaca-ore-samples-normalised-to-average-crustal-abundance.
Pals, D.W., Spry, P.G., Chryssoulis, S., 2003. Invisible gold and tellurium in arsenic rich pyrite from the Emperor gold deposit, Fiji: implications for gold distribution and deposition. Econ. Geol. 98, 479–493.
Parnell, J., Spinks, S., Brolly, C., 2018. Tellurium and selenium in Mesoproterozoic red beds. Precambr. Res. 305, 145–150. https://doi.org/10.1016/j.precamres.2017.12.022.
Plant, J.A., Bone, J., Voulvoulis, N., Kinniburgh, D.G., Smedley, P.L., Fordyce, F.M., Klinck, B., 2013. Arsenic and selenium. In: Treatise on Geochemistry: Second Edition. Elsevier, Amsterdam, Netherlands, 11, pp. 13–57.
Pohl, W., 2011. Economic Geology: Principles and Practice. Wiley-Blackwell Publishing, UK.
Rasmussen, B., Buick, R., 2000. Oily old ores: Evidence for hydrothermal petroleum generation in an Archean volcanogenic massive sulfide deposit. Geology 28 (8), 731–734.
Reich, M., Deditius, A., Chryssoulis, S., Li, J.-W., Ma, C.-Q., Parada, M.A., Barra, F., Mittermayr, F., 2013. Pyrite as a record of hydrothermal fluid evolution in a porphyr copper system: a SIMS/EMPA trace element study. Geochim. Cosmochim. Acta 104, 42–62.
Rovira, M., Giménez, J., Martínez, M., Martínez-Lladó, X., de Pablo, J., Martí, V., Duro, L., 2008. Sorption of selenium(IV) and selenium(VI) onto natural iron oxides: goethite and hematite. J. Hazard. Mater. 150 (2), 279–284.
Rudnick, R.L., Gao, S., 2014. Composition of the continental crust. In: Rudnick, R.L., (Ed.), The Crust (Revised Version), vol. 3. Elsevier, Amsterdam, The Netherlands, pp. 1–64.
Sandy, T., DiSante, C., 2010. Review of Available Technologies for the Removal of Selenium from Water; Technical Report; CH2M Hill: Englewood, CO, USA, June 2010; pp. 2–223.
Scheiber, T., Viola, G., Bingen, B., Peters, M., Solli, A., 2015. Multiple reactivation and strain localization along a Proterozoic orogen-scale deformation zone: the Kongsberg-Telemark boundary in southern Norway revisited. Precambr. Res. 265, 78–103.
Schirmer, T., Koschinsky, A., Bau, M., 2014. The ratio of tellurium and selenium in geological material as a possible paleo-redox proxy. Chem. Geol. 376, 44–51.
Simon, G., Kesler, S.E., Essene, E.J., 1997. Phase relations among selenides, sulfides, tellurides, and oxides: II. Applications to selenide-bearing ore deposits. Econ. Geol. 92, 468–484.
Spinks, S.C., Parnell, J., Bellis, D., Still, J., 2016. Remobilization and mineralization of selenium–tellurium in metamorphosed red beds: evidence from the Munster Basin, Ireland. Ore Geol. Rev. 72, 114–127.
Spinks, S.C., Parnell, J., Still, J.W., 2014. Redox-controlled selenide mineralization in the Upper Old Red Sandstone. Scott. J. Geol. 50, 173–182.
Starmer, I.C., 1977. The geology and the evolution of the southwestern part of the Kongsberg Series. Norsk Geologisk Tidsskrift 57, 1–22.
Starmer, I.C., 1985. The evolution of the South Norwegian Proterozoic as revealed by the major and mega-tectonics of the Kongsberg and Bamble sectors. In: Tobi, A.C., Tourets, J.L.R. (Eds.), The Deep Proterozoic Crust in North Atlantic Provinces. D. Reidel Publishing Company, Dordrecht, Netherlands, pp. 259–290.
Su, C., Suarez, D.L., 2000. Selenate and selenite sorption on iron oxides: An infrared and electrophoretic study. Soil Sci. Soc. Am. J. 64 (1), 101–111.
Sverdrup, T.L., Thorkildsen, C.D., Bjørlykke, H., 1967. Uran og thorium I Norge. Norges Geologiske Undersøkelse 250A, 1–31.
Tanner, D., Henley, R.W., Mavrogenes, J.A., Holden, P., 2016. Sulfur isotope and trace element systematics of zoned pyrite crystals from the El Indio Au-Cu-Ag deposit, Chile. Contrib. Miner. Petrol. 171 (4), 33-1-33-17.
Templeton, D.M., Ariese, F., Cornelis, R., Danielsson, L.G., Muntau, H., van Leeuwen, H.P., Lobinski, R., 2000. Guidelines for terms related to chemical speciation and fractionation of elements. Definitions, structural aspects, and methodological approaches (IUPAC Recommendations 2000). Pure Appl. Chem. 72 (8), 1453–1470.
TH Cresgate, 2016. Report on the Ore Mineralogy of Samples from the Lagoa Salgada, Volcanogenic Massive Sulphide (VMS) Deposit, Southern Portugal. Universidade Do Porto Petrographic Report LS-1.
Velbel, M.A., 1989. Weathering of hornblende to ferruginous products by a dissolution-reprecipitation mechanism: petrography and stoichiometry. Clays Clay Miner. 37 (6), 515–524.
Vikentev, I.V., 2006. Precious metal and telluride mineralogy of large volcanic-hosted massive sulfide deposits in the Urals. Mineral. Petrol. 87, 305–326.
Vikentev, I.V., 2016. Selenium, tellurium and precious metal mineralogy in Uchalinsk copper-zinc-pyritic district, the Urals. IOP Conf. Series. Mater. Sci. Eng. 123, 012027.
Vikentev, I., Seravkin, I., Moloshag, V., Skuratov, V., Yudovskaya, M., Mokhov, A., Kerzin, A., Tsepin, A., 2006. Au and Ag in ores of the Gaisk giant VHMS deposit, South Urals. 12th Quadrennial IAGOD Symposium, Moscow, Extended abstract CD-ROM, abstract 327, p. 5.
Vikentev, I.V., Yudovskaya, M.A., Mokhov, A.V., Kerzin, A.L., Tsepin, A.I., 2004. Gold and PGE in massive sulfide ore of the Uzelginsk deposit, Southern Urals, Russia. Can. Mineral. 42, 651–665.
Viola, G., Bingen, B., Solli, A., 2016. Berggrunnskart: Kongsberg litotektoniske enhet, Kongsberg–Modum–Hønefoss M 1:100 000. Norges Geologiske Undersøkelse.
Vogt, J.H.L., 1899. Über die Bildung des gedigenden Silbers, besonders des Kongsberger Silbers, durch Secundärprocesse aus Silberglanz und andren Silbererzen, und ein Versuch zur Erklärung der Edelheit der Kongsberger Gange an den Fahlbandkreuzen. Zeitschrift für praktische Geol. 133–177.
Wei, C., Bai, Y., Deng, A., Bao, Y., 2016. Universal synthesis of air stable, phase pure, controllable $FeSe_2$ nanocrystals. Nanotechnology 27, 165702 (9, pp).
White, A., Dubrovsky, M., 1994. Chemical oxidation–reduction controls on selenium mobility in groundwater systems. In: Frankenberger, W.T., Benson, S. (Eds.), Selenium in the Environment. Marcel Dekker, New York, pp. 185–222.
Xiong, Y.L., 2003. Predicted equilibrium constants for solid and aqueous selenium species to 300 °C: applications to selenium-rich mineral deposits. Ore Geol. Rev. 23, 259–276.